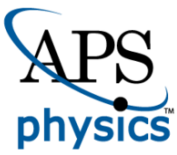

Plasmon dissipation in gapped graphene open systems at finite temperature

Andrii Iurov, Godfrey Gumbs, Danhong Huang, and V. M. Silkin

Phys. Rev. B **93**, 035404 — Published 4 January 2016

DOI: 10.1103/PhysRevB.93.035404

Plasmon dissipation in gapped-graphene open systems at finite temperature

Andrii Iurov[1], Godfrey Gumbs[2,3], Danhong Huang[4,1], and V. M. Silkin[3]
[1] *Center for High Technology Materials, University of New Mexico, Albuquerque, NM 87106, USA*
[2] *Department of Physics and Astronomy, Hunter College of the City University of New York, 695 Park Avenue, New York, NY 10065, USA*
[3] *Donostia International Physics Center (DIPC), P de Manuel Lardizabal, 4, 20018, San Sebastian, Basque Country, Spain*
[4] *Air Force Research Laboratory, Space Vehicles Directorate, Kirtland Air Force Base, NM 87117, USA*
(Dated: December 15, 2015)

Numerical and closed-form analytic expressions for plasmon dispersion relations and rates of dissipation are first obtained at finite-temperatures for free-standing gapped graphene. These closed-system results are generalized to an open system with Coulomb coupling of graphene electrons to an external electron reservoir. New plasmon modes, as well as new plasmon dissipation channels, are found in this open system, including significant modifications arising from the combined effect of thermal excitation of electrons and an energy bandgap in gapped graphene. Moreover, the characteristics of the new plasmon mode and the additional plasmon dissipation may be fully controlled by adjusting the separation between the graphene layer from the surface of a thick conductor. Numerical results for the thermal shift of plasmon frequency in a doped gapped graphene layer, along with its sensitivity to the local environment, are demonstrated and analyzed. Such phenomenon associated with the frequency shift of plasmons may be applied to direct optical measurement of local electron temperature in transistors and nanoplasmonic structures.

PACS numbers: 73.21.-b, 71.70.Ej, 71.45 Gm, 73.20.Mf

I. INTRODUCTION

Plasmon excitations in graphene are one of the most exciting and actively studied subjects both theoretically [1–7] and experimentally [8–12]. Graphene plasmons are especially important, partially because of their versatile frequency range tuned by varying doping concentration and energy band gap. Consequently, graphene is expected to have several potential device applications in transistors, optics, microscopy and nanolithography [13–15]. These studies on graphene plasmonics also extend to other carbon-based structures, such as fullerenes [16–21], carbon nanotubes [22,23], and especially recently discovered silicon-based silicene and other buckled honeycomb lattice structures [24,25] with on-site potential differences between sublattices.

It is well known that the dynamics of self-sustaining density oscillations (i.e., plasmons) in a closed system may be very well described by Dyson's equation in many-body theory for two-particle Green's functions, from which both the plasmon dispersion relation and the intrinsic plasmon dissipation rate (inverse quasiparticle lifetime) may be determined [6]. For an open system [26–33], on the other hand, the dynamics for carrier excitations is much more complicated and will strongly depend on the electronic coupling to its environment (external reservoir). Open-system dynamics (both classical and quantum) includes tunnel-coupling of a conductor to external electrodes [34], leakage-of an optical cavity to free space [35], and thermal coupling of an electronic system to a heat bath [36]. The coupling to an external reservoir will introduce additional dissipation channels for an electronic system, in addition to an extra contribution for internal electron interactions. Such energy-dissipation dynamics in an open system has been treated in the past using the so-called Lindblad dissipative superoperator [37].

Although the plasmon dynamics in free-standing monolayer graphene- (closed system) has been explored extensively, there are much fewer optical studies for graphene coupled by Coulomb interaction to an external electron reservoir [38]. The existence of such an reservoir will introduce Coulomb coupling between the graphene electrons and those carriers in a conducting substrate, as illustrated in our proposed nanoscale hybrid structure in Fig. 1. Dielectric screening of the electron-electron interaction within the graphene layer will be modified by their coupling to the reservoir, thereby leading to a new plasmon mode as well as a new dissipation channel concurrently [37]. Moreover, introduction of an energy gap in monolayer graphene as well as thermal excitations of electrons at finite temperatures, will further modify this Coulomb coupling to the reservoir. The main application of the current study aims to establish a basic principle for a contactless measurement of local electron temperature. One way for non-invasive measurement of local electron temperature [39–43] is based on the thermal shift of plasmon energies, including the effects of graphene coupling to an external electron source.

One of our goals in this paper is to investigate the effects of an energy band gap and temperature on the plasmon excitation energy dispersion and dissipation in doped monolayer graphene. Specifically, we investigated different

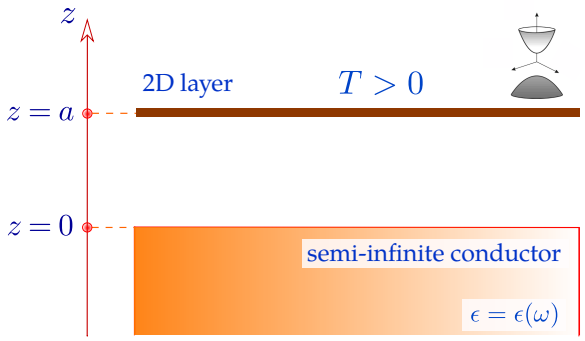

FIG. 1: (Color online) Schematics of a graphene-based hybrid structure (open system), which consists of a gapped graphene layer coupled by Coulomb interaction to a semi-infinite conducting substrate (electron reservoir). The graphene layer is embedded in a dielectric material (not shown) and separated by distance a from the surface. The dielectric constant of the host material is $\epsilon_s = 4\pi\epsilon_0\epsilon_b$ with a relative dielectric constant $\epsilon_b = 2.4$.

dynamics of graphene electrons for the cases when either the graphene layer is free-standing (closed system) or when it is in close proximity with a thick conducting substrate (treated as an electron reservoir in an open system). The dissipation of plasmons is associated with Landau damping by particle-hole modes, which will be modified by the Coulomb coupling of graphene electrons to an adjoining system in addition to the shift of the plasmon frequency. Considering the fact that finite temperatures may also induce plasmon dissipation into particle-hole pairs, we have investigated how this reservoir-related dissipation rate depends on temperature.

Closed-form analytic expressions for the long-wavelength plasmon dispersion relation in gapped graphene as well as the dynamical polarization function at zero temperature were reported by Pyatkovskiy in Ref. [3]. This important study predicted the existence of dissipation-free plasmons in a large range of wave vector in the presence of a finite energy gap. Such a bandgap can be opened by either using a substrate or by illuminating graphene with circularly-polarized light. [44] The polarization function for gapped graphene in this case was derived analytically in Ref. [45].

In order to tailor effectively the plasmon frequencies, graphene has been hybridized with prefabricated plasmonic nanoarrays and metamaterials [46–48]. Therefore, a thorough understanding of the dispersion and dissipation of plasmons in graphene interfacing with different kinds of substrates is necessary for designing innovative devices and their applications. In this paper, we investigate finite-temperature nonlocal-plasmon dynamics in a graphene open system which includes Coulomb-coupling to an electron reservoir (semi-infinite conducting substrate). Here, we concentrate on the dynamics of energy dissipations for both surface-plasmon-like (upper) and graphene-like (lower) [10,38] branches and their energy renormalization by finite temperatures.

The rest of the paper is organized as follows. In Sec. II, as an example for the closed system, we generalized the polarization function for gapless graphene in Ref. [4] to one for gapped graphene at finite temperature, in which the analytical expressions for plasmon dispersion and dissipation rate are derived for both the low- and high-temperature limits. In Sec. III, we formulate the Coulomb coupling of graphene electrons to an external electron reservoir. Furthermore, the renormalization of graphene plasmon dispersion, as well as the additional plasmon dissipation channel, by interacting with a reservoir are investigated and associated numerical results are presented in Sec. IV, including effects of finite temperatures and energy gaps. Finally, some concluding remarks are presented in Sec. V.

II. PLASMONS IN GAPPED-GRAPHENE LAYERS AT FINITE TEMPERATURE

To elucidate clearly the physics of plasmon excitations in proposed gapped-graphene based hybrid structures, as shown in Fig. 1, the natural first step in this study is to calculate analytically the plasmon modes in gapped graphene at finite temperature by neglecting its interaction with the conducting substrate, thereby treating it as a closed quantum system. In this case, the plasmon dissipation is entirely determined by the material properties, wave number and temperature, and the plasmons are determined by the zeros of the dielectric function $\epsilon_T(q,\omega;\,\mu) = 1 - V(q)\,\Pi_T^{(0)}(q,\omega;\mu)$. Here $V(q) = 2\pi e^2/\epsilon_s q$ is the Coulomb interaction for a two-dimensional (2D) layer. Also ϵ_s is the dielectric constant of graphene two-dimensional layer. It is defined as $\epsilon_s = 4\pi\epsilon_0\,\epsilon_b$, where ϵ_0 is the permeability of free space and ϵ_b is the background dielectric constant. For all our numerical calculations in this paper, we take $\epsilon_b = 2.4$.

We begin with the non-interacting electron polarizability at zero temperature, given by [1,2,49,50]

$$\Pi^{(0)}_{T=0}(q,\omega;\,E_F) = -\frac{gg'}{4\pi^2}\int d^2\mathbf{k}\, f^{ss'}(\mathbf{q},\mathbf{k})\,\frac{n_{T=0}[\varepsilon_s(k)-E_F]-n_{T=0}[\varepsilon_{s'}(|\mathbf{k}+\mathbf{q}|)-E_F]}{\varepsilon_s(k)-\varepsilon_{s'}(|\mathbf{k}+\mathbf{q}|)+\hbar(\omega+i\gamma)}\ . \tag{1}$$

Here, we have $g=2$ for spin degeneracy and $g'=2$ for valley degeneracy. Also, E_F is the Fermi energy at zero temperature, $\varepsilon_s(k)=s\sqrt{\Delta^2+(\hbar v_F k)^2}$ denotes the energy dispersion for the $s=1$ (electron-like) and $s=-1$ (hole-like) subbands, where 2Δ is the energy gap and v_F is the Fermi velocity in pristine graphene. The occupation factors of an electron state $|\mathbf{q},s\rangle$ are given by the Fermi-Dirac distribution functions. Finally, the form factor $f^{ss'}(\mathbf{q},\mathbf{k}) = |\langle\mathbf{q}+\mathbf{k},s'|\mathsf{e}^{i\mathbf{q}\cdot\mathbf{r}}|\mathbf{k},s\rangle|^2$.

We now turn to a derivation of the finite-temperature polarization function $\Pi^{(0)}_T(q,\omega;\,\mu)$ for gapped graphene. It has been noted [4,51,52] that the desired polarizability could be obtained as an integral transformation of its corresponding zero-temperature value $\Pi^{(0)}_{T=0}(q,\omega;\,E_F)$:

$$\Pi^{(0)}_T(q,\omega;\,\mu) = \frac{\beta}{2}\int_0^\infty dE\ \frac{\Pi^{(0)}_{T=0}(q,\omega;\,E)}{1+\cosh\left[\beta(\mu-E)\right]}\ , \tag{2}$$

where $\beta=1/k_BT$ and $\mu(T)$ is the electron chemical potential at temperature T.

An important difference in the calculation of the polarizability for the presence of the gap in graphene is that we must exclude electron energies below the gap $|\varepsilon|<\Delta$, which means that we need to introduce another Heaviside step $\theta(|\varepsilon|-\Delta)$ besides the actual distribution function. This is essential in comparison with gapless graphene or the 2D electron gas. This situation has been considered in the calculation of the zero-temperature polarizability by setting the proper limits for k-integrals [3]. One may easily verify that $\theta(|\varepsilon|-\Delta)$ also accounts for the temperature dependence of the chemical potential $\mu(T)$ as well as the doping dependance at a given temperature used in Eq. (2).

A. Low-Temperature Limit

We first consider the low-temperature limit with $k_BT \ll E_F$ (or $k_BT \ll \hbar\omega$ for intrinsic graphene) in the polarization function. For $T\to 0$, the integration kernel which also includes factor β outside the integral in Eq. (2) becomes a delta function, scaled as $\beta\mathsf{e}^{-\beta|\mu-E|}$ diverging at $E=\mu$. By assuming that the μ-dependence of the polarization is smooth for a low enough temperature, one may expand $\Pi^{(0)}_T(q,\omega;\,\mu)$ in a power series. As a result, we arrive at the following expression

$$\Pi^{(0)}_T(q,\omega;\,\mu) = \Pi^{(0)}_{T=0}(q,\omega;\,\mu) + \frac{\pi^2}{24}\,(k_BT)^2\,\frac{\partial^2}{\partial\mu^2}\Pi^{(0)}_{T=0}(q,\omega;\,\mu)\ . \tag{3}$$

We emphasize that the temperature-dependent chemical potential μ enters this result because we expanded the hyperbolic cosine function in Eq. (2) around $E=\mu$ so that even the first term on the right-hand side of Eq. (3) depends on temperature. We now exploit Eq. (3) for gapped graphene in the long wavelength limit with the help of [3]

$$\Pi^{(0)}_{T=0}(q\ll k_F,\omega;\,\mu) = \frac{\mu}{\pi\hbar^2}\left[1-\left(\frac{\Delta}{\mu}\right)^2\right]\,\frac{q^2}{\omega^2}\ , \tag{4}$$

where k_F is the Fermi wave number for gapped graphene. This expression is valid only for extrinsic graphene with $E_F>\Delta$. Consequently, the polarization function becomes

$$\begin{aligned}\Pi^{(0)}_T(q,\omega;\mu) &= I(T)\,\frac{q^2}{\omega^2}\\ I(T) &= \frac{\mu}{\pi\hbar^2}\left[1-\frac{\Delta^2}{\mu^2}-\frac{\pi^2}{12}\,\frac{\Delta^2}{\mu^4}(k_BT)^2\right]\ .\end{aligned} \tag{5}$$

The corresponding plasmon dispersion relation is $\omega_p^2(q) = (2\pi e^2/\epsilon_s)\, I(T)\, q$. We conclude that the plasmon frequency is lowered, in comparison with the result with a bandgap at zero temperature. However, the $\backsim q^{1/2}$ dispersive feature is still preserved, as for all 2D materials. Since the density of states $D(\varepsilon)$ of graphene is unchanged in the presence of an energy gap, and given by $D(\varepsilon) = 2\varepsilon/(\pi\hbar^2 v_F^2)$, as well as the chemical potential $\mu(T)$ at low temperatures ($T \ll T_F$) is calculated as $\mu(T)/E_F \backsim 1 - (\pi^2/6)\,(T/T_F)^2$, the polarization function may be expressed through the zero-temperature Fermi energy as

$$\Pi_T^{(0)}(q,\omega;\,\mu) = \left[\frac{(E_F^2 - \Delta^2)}{\pi\hbar^2 E_F} - \pi\,\frac{2E_F^2 + 3\Delta^2}{12\hbar^2 E_F}\,\left(\frac{T}{T_F}\right)^2\right]\frac{q^2}{\omega^2}\;, \tag{6}$$

where $T_F = E_F/k_B$ is the Fermi temperature.

B. High-Temperature Limit

Turning now to the high-temperature limit for the polarization function for gapped graphene, we still start with the integral transformation in Eq. (2) and the zero-temperature polarization function in Eq. (4) in the long-wavelength limit. These results are regarded as a generalization of the zero-temperature plasmons in gapped graphene [3] as well as the finite temperature polarization function in graphene with no gap [4]. Our analytical calculations for intrinsic graphene ($\mu = 0$) yield (see details in Appendix A)

$$\mathrm{Re}\,\Pi_T^{(0)}(q,\,\omega;\,\mu=0) = \frac{g_t \ln 2}{2\pi}\frac{q^2}{\hbar^2\omega^2}\,k_B T - \frac{g_t}{4\pi\hbar^2}\,\frac{\Delta^2}{4k_B T}\left[\mathbb{C} - \ln\left(\frac{\Delta}{2k_B T}\right)\right]\frac{q^2}{\omega^2}\;, \tag{7}$$

where $g_t = gg' = 4$ is the total degeneracy factor of graphene electrons and $\mathbb{C} \approx 0.8$ is a small positive constant (see detailed evaluations of $\mathbb{C}$ in Appendix A). Consequently, we obtain the plasmon dispersion relation as

$$\omega_p^2(q) = \frac{4}{\hbar}\,v_F r_s q\left\{k_B T \ln 2 - \frac{\Delta^2}{8k_B T}\left[\mathbb{C} - \ln\left(\frac{\Delta}{2k_B T}\right)\right]\right\}\;, \tag{8}$$

where $r_s = e^2/\epsilon_s\hbar v_F$ is the so-called graphene fine-structure constant.

The dissipation rate $\gamma(q,\,T;\,\mu)$ (inverse lifetime) for the case of weak dissipation is defined as

$$\gamma(q,\,T;\,\mu) = \frac{\mathrm{Im}\,\Pi_T^{(0)}(q,\omega=\omega_p;\,\mu)}{\dfrac{\partial}{\partial\omega}\mathrm{Re}\,\Pi_T^{(0)}(q,\omega;\,\mu)\Big|_{\omega=\omega_p}}\;, \tag{9}$$

where the evaluation of the plasmon dispersion $\omega = \omega_p(q)$ is a prerequisite for calculating $\gamma(q,\,T;\,\mu)$. $\omega = \omega_p(p)$ is in reference to the real plasmon frequency obtained as solutions of the real part of the dielectric function, i.e.,

$$\mathrm{Re}\,\epsilon_T(q,\,\omega_p;\,\mu) = 1 - V(q)\,\mathrm{Re}\,\Pi_T^{(0)}(q,\,\omega_p;\,\mu) = 0\;. \tag{10}$$

Eq. (9) appears as consequence of the series expansion of the polarizability (both real and imaginary parts) with respect to a small damping parameter $\gamma(q)$.

The imaginary part of the zero-temperature polarization function is given by [3]

$$\mathrm{Im}\,\Pi_{T=0}^{(0)}(q,\omega;\,E_F) = \frac{g_t q^2}{8\hbar\omega}\left(1 - \frac{1}{2}X_0^2\right)\theta(\hbar\omega - 2E_F)\;, \tag{11}$$

where

$$X_0 = \sqrt{1 + \frac{4\Delta^2}{\hbar^2\,(v_F^2 q^2 - \omega^2)}} \backsim 1 - \frac{2\Delta^2}{\hbar^2\omega^2}\;, \tag{12}$$

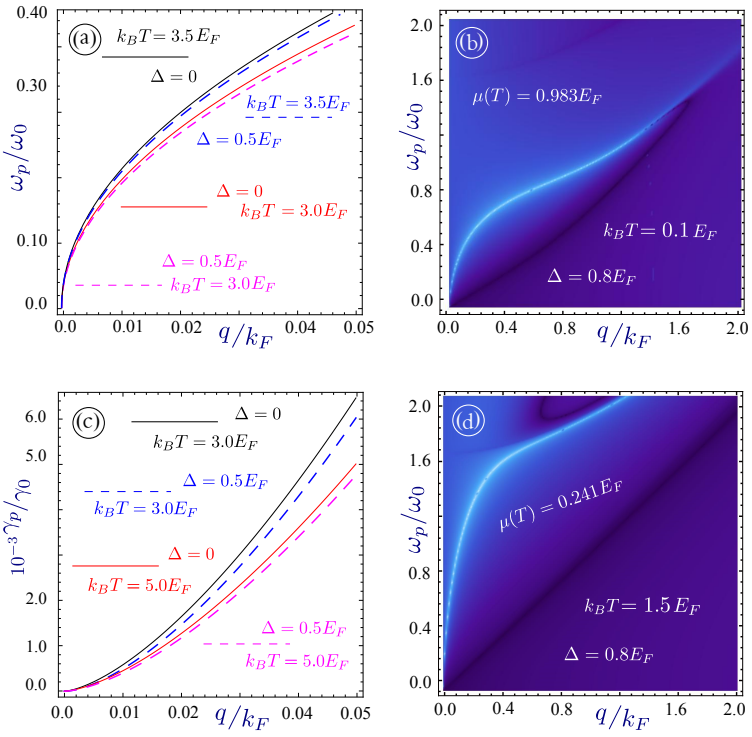

FIG. 2: (Color online) Analytical (left) and numerical (right) results for plasmons in gapped graphene. Panels (a), (c) represent respectively the analytical plasmon dispersions and dissipation rates of intrinsic graphene in the long-wavelength limit. Plot (a) shows the plasmon frequency ω_p in units of $\omega_0 = (2E_F/\hbar)\sqrt{\ln 2}$, where $E_F = \hbar v_F k_F = 0.05\,\text{eV}$, while plot (c) displays the dissipation rate γ_p in units of $\gamma_0 = (\pi E_F/8\hbar)\sqrt{r_s^3 \ln 2}$ for the case of high temperatures. Different values of Δ and k_BT are individually labeled in plots (a), (c). The numerical calculations of plasmon dispersions are presented in panels (b), (d) for two temperatures $k_BT/E_F = 0.1$, 1.5 as well as a fixed energy gap $\Delta/E_F = 0.8$.

which gives

$$\text{Im}\,\Pi^{(0)}_{T=0}(q,\omega;\,E_F) = \frac{g_t q^2}{16\hbar\omega}\left(1+\frac{4\Delta^2}{\hbar^2\omega^2}\right)\theta(\hbar\omega - 2E_F)\;. \tag{13}$$

By using Eq. (2), the imaginary part of the finite-temperature polarizability of intrinsic graphene is obtained as

$$\text{Im}\,\Pi^{(0)}_{T}(q,\omega;\,\mu=0) = \frac{g_t q^2}{16\hbar\omega}\left(1+\frac{4\Delta^2}{\hbar^2\omega^2}\right)\int_{\Delta}^{\infty}\frac{d\,\mu'}{4k_BT}\frac{\theta(\hbar\omega-2\mu')}{\cosh^2(\mu'/2k_BT)} = \frac{g_t}{64}\frac{q^2}{k_BT}\left(1-\frac{\Delta}{\hbar\omega}\right)\;. \tag{14}$$

Consequently, using Eq. (9), we obtain the lowest-order linear correction $\backsim\ \Delta$ to the dissipation rate in intrinsic gapped graphene as

$$\gamma(q,\,T;\,\mu=0) = \frac{\pi}{8}\sqrt{\frac{\hbar}{k_BT}}(\ln 2)^{1/2}(r_s v_F)^{3/2}q^{3/2} - \frac{\pi}{16}\,r_s v_F q\left(\frac{\Delta}{k_BT}\right)\;. \tag{15}$$

From our calculated dissipation rate we find that the existence of a bandgap will slow down the plasmon dissipation.

The plasmon dispersion relation determined by the change in the density plot peaks with q and the associated dissipation rates proportional to the brightness of these peaks for gapped graphene are presented in Fig. 2 for chosen values of T, E_F and Δ using the numerically obtained temperature dependence of the chemical potential based on the results of Ref. [53]. The plasmon frequencies ω_p increase with temperature T in Fig. 2(a), scaled as $\backsim\sqrt{T}$ in the long wavelength limit. On the other hand, the energy gap slightly reduces ω_p in the same plot at high temperatures. Therefore, there is interplay between thermal and bandgap effects with respect to ω_p. The dissipation rate γ_p of

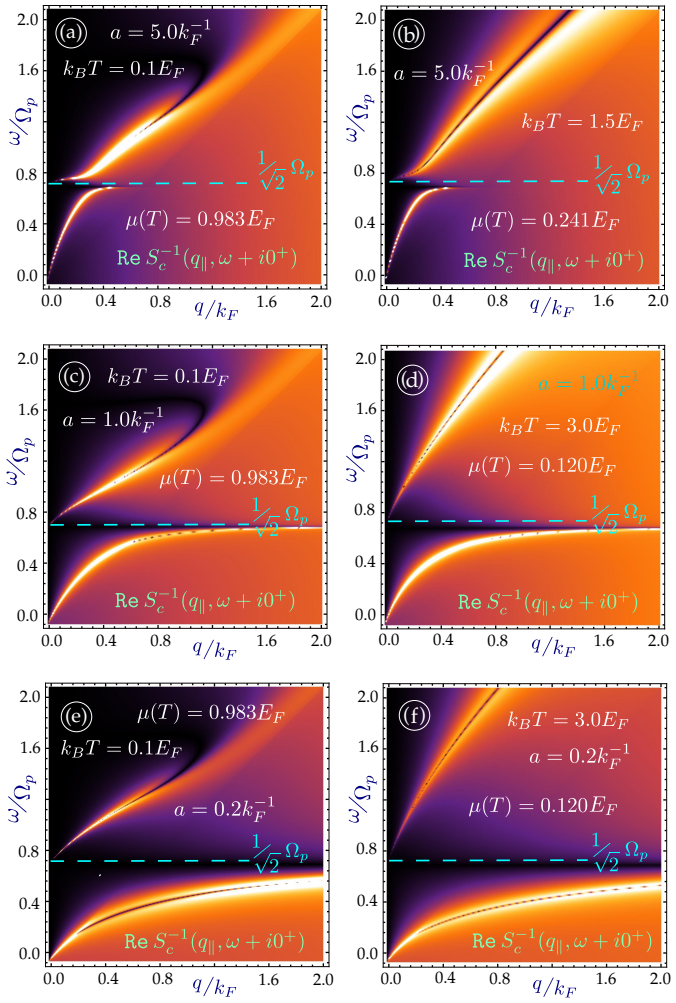

FIG. 3: (Color online) Density plots of the real part of $S_C(q, \omega + i0^+)$ for $\Delta = 0$ and doped graphene at chosen temperatures. Peaks of these plots correspond to the plasmon resonances for various values of T and a. Here, $E_F = \hbar v_F k_F = 10\,\text{meV}$, for the electron density $n = 10^{14}\,\text{m}^{-2}$. Plots in (a), (c), (e) are for $k_BT = 0.1\,E_F$, while those in (b), (d), (f) for $k_BT = 1.5\,E_F$. Additionally, panels (a), (b) are for $a = 5.0\,k_F^{-1}$, but those of (c), (d) to $a = 1.0\,k_F^{-1}$. Panels (e), (f) correspond to $a = 0.2\,k_F^{-1}$.

plasmons is determined by the particle-hole mode damping. As shown in Figs. 2(b) and 2(d), the increase of T leads to an expansion of the intraband single-particle excitation region below the main diagonal in the $\omega - q$ space. Furthermore, the interband particle-hole mode region is extended and leads to considerable Landau damping of the upper plasmon branch above the main diagonal at $k_BT = 1.5\,E_F$. However, in the high-temperature limit with $k_BT \gg \hbar v_F q$ and $k_BT \gg \Delta$, these interband particle-hole modes are suppressed, leading to significantly reduced γ_p in Fig. 2(c). Also from Fig. 2(c), it is interesting to notice the decrease of γ_p with increasing Δ at intermediate temperatures. Another distinct feature in Fig. 2(d) is that for large energy gap $\Delta/E_F = 0.8$ and $k_BT = 1.5\,E_F$, the plasmon mode is kept undamped for a relatively wider q-range within the gap region between the interband and intraband particle-hole modes.

III. PLASMONS IN OPEN GRAPHENE-BASED HYBRID SYSTEMS AT FINITE TEMPERATURE

In Sec. II, graphene was assumed to be embedded in the surrounding host dielectric material, making it possible to be treated as a closed quantum system. However, when the graphene layer is brought close to a conducting medium, the Coulomb interaction between graphene and the nearby conductor cannot be neglected and the hybrid graphene system should be regarded as an open system. Physically, graphene is a single atomic-layer material, which implies that it will inevitably interact with its embedding host or adjoining conducting substrate. In considering monolayer graphene on the surface of a conductor as an example for open systems, we introduce additional plasmon dissipation

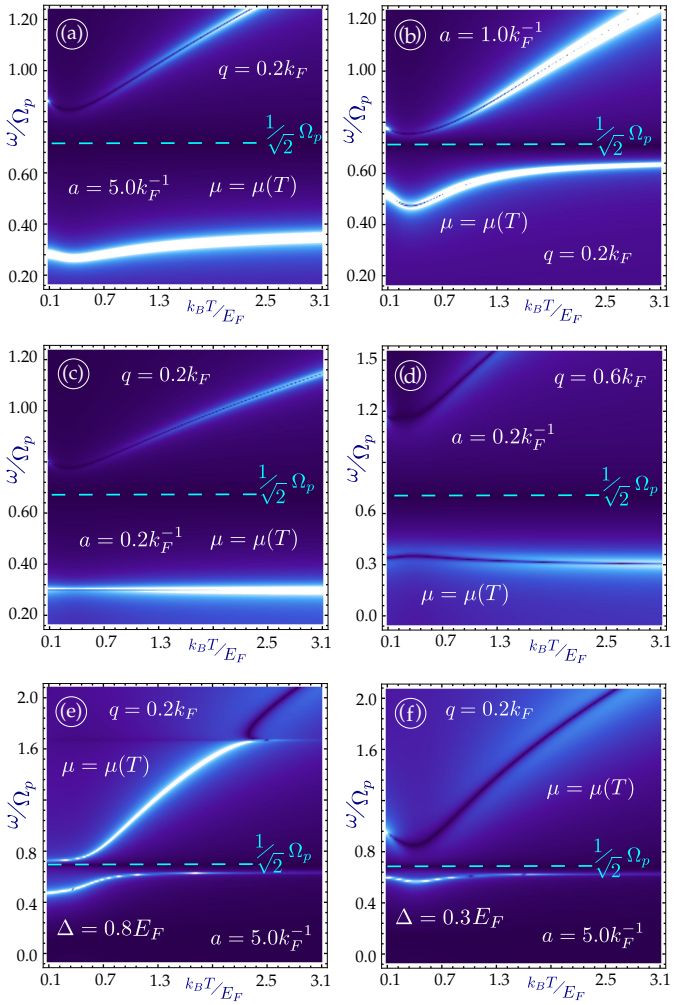

FIG. 4: (Color online) Density plots of the real part of $S_C(q, \omega + i0^+)$ as functions of T for doped graphene for two values of q. Panels (a)-(d) are for $(\Delta = 0)$, while panels (e), (f) for different energy bandgaps. All plots are shown for $q = 0.2\,k_F$ except plot (d) for $q = 0.6\,k_F$. In addition, panels (a), (e), (f) display results for well-separated graphene layer with $a = 5.0\,k_F^{-1}$, while panels (b), (c) for $a = 0.2\,k_F^{-1}$ and (d) for $a = 1.0\,k_F^{-1}$. Here, $E_F = 10\,\text{meV}$ is chosen.

channels due to the Coulomb interaction between electrons in graphene and the substrate which we model as an electron liquid. Such an arrangement makes electronic excitation in a graphene layer sensitive to changes in their environment, including the presence of a single molecule, electron doping, and even thermal fluctuations.

A. Interaction with Electron Reservoir

By including the Coulomb interaction between graphene and the conducting substrate, the nonlocal inverse dielectric function of such an open system $\mathcal{K}(z_1, z_2)$ satisfies the following equation as described in Refs. [38,54]

$$\mathcal{K}(z_1, z_2) = K_S(z_1, z_2) + \Pi_T^{(0)}(q, \omega; \mu)\, \frac{K_S(a, z_2)}{S_C(q, \omega; \mu)} \left\{ \int_{-\infty}^{\infty} dz'\, K_S(z_1, z')\, v_C(q, z' - a) \right\} , \tag{16}$$

where $K_S(z_1, z_2)$ denotes the nonlocal inverse dielectric function of the semi-infinite conducting substrate with

$$K_S(z,\, z'|q,\, \omega) \;\; = \theta(z)\left\{\delta(z-z') + \delta(z')\, e^{-qz}\left[\frac{1-\epsilon_B(\omega)}{1+\epsilon_B(\omega)}\right]\right\} + \theta(-z)\left\{\frac{\delta(z-z')}{\epsilon_B(\omega)} + \delta(z')\, e^{qz}\,\frac{1}{\epsilon_B(\omega)}\left[\frac{\epsilon_B(\omega)-1}{\epsilon_B(\omega)+1}\right]\right\}\,, \tag{17}$$

and $z > 0$ ($z < 0$) corresponds to air (conductor) side, respectively, with the surface at $z = 0$. Also, $\epsilon_B(\omega) = 1-\Omega_p^2/\omega^2$ is given by the Drude model for an electromagnetic coupling with Ω_p being the bulk plasma frequency. Here, $\Omega_p = \sqrt{n_0 e^2/\epsilon_0\epsilon_r m^*}$, where n_0, ϵ_r and m^* are the bulk free-carrier concentration, dielectric constant and carrier effective mass, respectively. Free-carrier concentration n_0 of a conductor can vary by many orders of magnitude from metals to doped semiconductors. Consequently, the bulk plasmon energy $\hbar\Omega_p$ in a conductor can change over a wide range from 10 meV to several eV. On the other hand, ϵ_b can also be changed up to two orders of magnitude by selecting different conducting materials, such as Bi_2Se_3[55,56].

Dielectric function $\epsilon_B(\omega)$ for the conducting substrate was treated in the local approximation in our numerical calculations, with no wave vector dependence or damping, while the $K_S(z_1; z_2)$ is referred to as "nonlocal" because it includes the exponential q-dependent Coulomb coupling between the graphene and the conducting substrate in the z-direction as shown in Eq. (17). In addition, the nonlocal q dependence can be added to the local form $\epsilon_B(\omega)$ by using a hydrodynamic model.

Non-locality and damping of the plasmon in the conducting substrate may also be introduced by going beyond the local approximation for the bulk dielectric function. This nonlocal treatment The bulk plasma frequency Ω_p is a crucial parameter for our hybridized plasmons, whose role is to determine the frequency and exact behavior of the coupled plasmon modes at various temperatures. Consequently, in order to make the coupling effect observable, we must ensure that the frequencies of the two plasmon modes (surface plasmon in the conducting substrate and the plasmon and Fermi energy in the two-dimensional layer, e.g. graphene) should be of the same order of magnitude. Apart from this, it is useful to keep track of the plasmon damping which appears if the collective modes enter the regions of single-particle excitations. In this sense, the frequency Ω_p directly affects Landau damping of each mode.

The interaction between graphene and the substrate is included in the second term of Eq. (16), a is the distance of the graphene layer from the conducting surface, $v_C(q,\, z-z') = (2\pi e^2/\epsilon_s)\, \exp(-q|z-z'|)$, and

$$S_C(q,\omega;\,\mu) = 1 - \frac{2\pi e^2}{\epsilon_s q}\,\Pi_T^{(0)}(q,\omega;\,\mu)\left\{1 + e^{-2qa}\,\frac{1-\epsilon_B(\omega)}{1+\epsilon_B(\omega)}\right\}\,. \tag{18}$$

The denominator $S_C(q,\omega;\,\mu)$ in Eq. (16) yields the poles in the inverse dielectric function and consequently the plasma dispersion relation.

B. Gapless Graphene

For open systems, we know from Lindhard's theory that the interaction of a graphene layer with a conducting substrate will not only acquire additional interaction for plasmons, as presented in Eq. (18), but also introduce more dissipation channels for plasmons. Here, the surface plasmon dissipation into an electron reservoir will be neglected. This is reasonable for a large range of wave vectors $q \ll 1/\lambda_F$, where $\lambda_F \backsimeq 0.5\, nm$ is the Fermi wavelength in metals comparable with the lattice constant. It has already been shown that Landau damping of plasmons plays a crucial role on the high-temperature dispersion relations. Therefore, we expect the Landau damping of graphene plasmons at high temperatures will be further modified by its interaction with conducting substrate. Another factor which may contribute to dissipation includes energy gap opening in a graphene layer. As reported previously, $\backsim 0.1$ eV energy gap in graphene could be created not only by a substrate, but also by irradiation using circularly-polarized light [44]. Polarization function, plasmons and their dissipation in this case were addressed in Ref. [45].

As an illustration of dissipation physics, we take the graphene polarizability with $\Delta = 0$ in the long-wavelength limit, as given in Ref. [4] and Eq. (7), and obtain

$$1 - \frac{2\pi}{q}\,\hbar r_s v_F\,\frac{2\ln 2}{\pi\hbar^2}\,\frac{q^2}{\omega^2}\,k_B T\left\{1 + \mathsf{e}^{-2qa}\,\frac{\Omega_p^2}{2\omega^2-\Omega_p^2}\right\} = 1 - q\Lambda_0(T)\left(\frac{\Omega_p}{\omega}\right)^2\left\{1 + \mathsf{e}^{-2qa}\,\frac{1}{2(\omega/\Omega_p)^2-1}\right\} = 0\,, \tag{19}$$

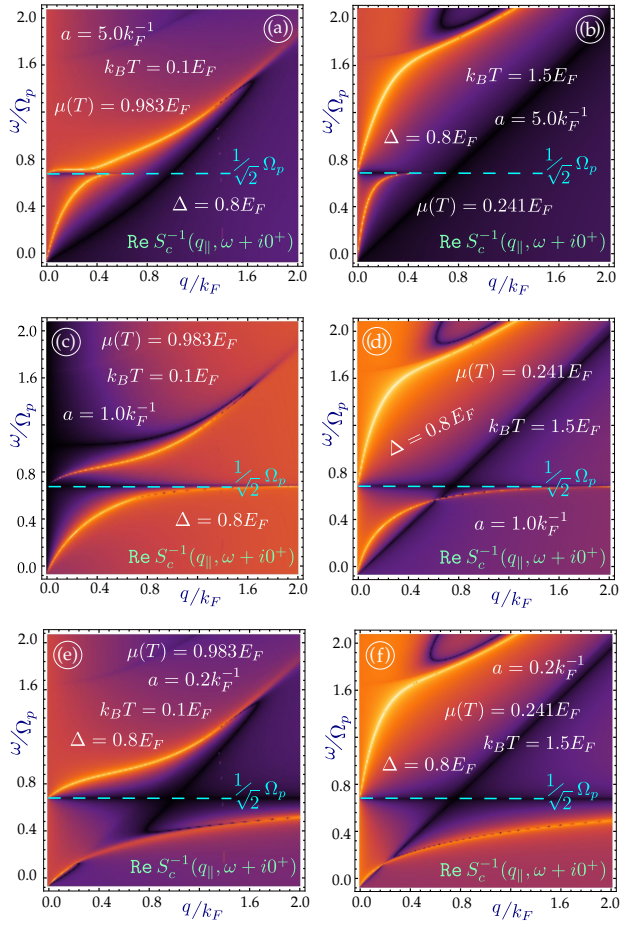

FIG. 5: (Color online) Density plots of the real part of $S_C(q, \omega + i0^+)$ with a large energy gap $\Delta = 0.8\,E_F$ at finite T for various values of a and T. Panels (a), (c), (e) correspond to a lower temperature with $k_BT = 0.1\,E_F$, while panels (b), (d), (f) to a higher temperature $k_BT = 1.5\,E_F$. Additionally, smaller layer separations are chosen with $a = 5.0\,k_F^{-1}$ in plots (a), (b), $a = 1.0\,k_F^{-1}$ in plots (c), (d) and $a = 0.2\,k_F^{-1}$ in plots (e), (f), respectively. Here, $E_F = 10\,\mathrm{meV}$ is taken.

where $\Lambda_0(T) = 4\ln 2\,(r_s v_F/\hbar\Omega_p^2)\,k_BT$ playing the role of "effective length" in the plasmon dispersion $\backsim \sqrt{q\Lambda_0(T)}$.

We consider first the case which corresponds to small layer separation or $qa \ll 1$. For this, we find in the linear approximation

$$\begin{aligned} \omega_{p,1}(q) &= \sqrt{8\ln 2\,\frac{r_s v_F}{\hbar}}\,\sqrt{a}\,\sqrt{k_BT}\,q\;, \\ \omega_{p,2}(q) &= \frac{\Omega_p}{\sqrt{2}} + \sqrt{8}\ln 2\,\frac{r_s v_F}{\hbar\,\Omega_p}\,k_BT\,q\;. \end{aligned} \tag{20}$$

Both branches are linear in q, and the surface plasmon $\omega_{p2}(q)$ does not depend on a in this approximation.

In the limit when $qa \gg 1$, a straightforward calculation yields

$$\begin{aligned} \omega_{p,1}(q) &= \Omega_p\sqrt{q\Lambda_0(T)} - \frac{\Omega_p\sqrt{q\Lambda_0(T)}}{2[1-2q\Lambda_0(T)]}\,\mathrm{e}^{-2qa}\;, \\ \omega_{p,2}(q) &= \frac{\Omega_p}{\sqrt{2}} + \frac{q\Lambda_0(T)\Omega_p}{\sqrt{2}[1-2q\Lambda_0(T)]}\,\mathrm{e}^{-2qa}\;. \end{aligned} \tag{21}$$

In addition, within the usual limit of $q\Lambda_0(T) \ll 1$, we have $1 - 2q\Lambda_0(T) \approx 1$ and obtain from Eq. (21)

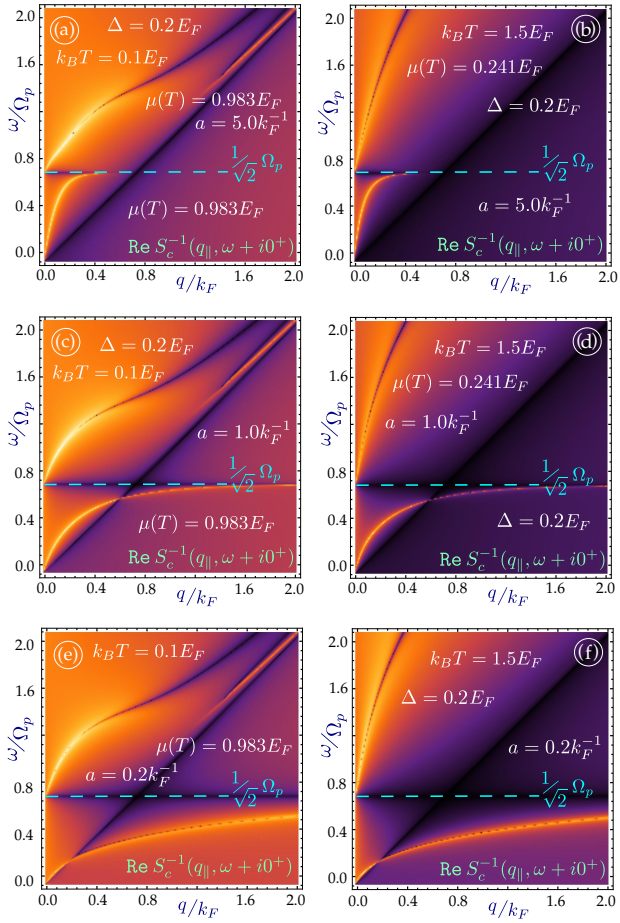

FIG. 6: (Color online) Density plots of the real part of $S_C(q, \omega + i0^+)$ with a large energy gap $\Delta = 0.2\,E_F$ at finite T for various values of a and T. Panels (a), (c), (e) are for a lower temperature $k_BT = 0.1\,E_F$, while panels (b), (d), (f) for a higher temperature $k_BT = 1.5\,E_F$. Moreover, different layer separations are taken for $a = 5.0\,k_F^{-1}$ in plots (a), (b), $a = 1.0\,k_F^{-1}$ in plots (c), (d) and $a = 0.2\,k_F^{-1}$ in plots (e), (f), respectively. Here, $E_F = 10\,\mathrm{meV}$ is chosen.

$$\begin{aligned}
\omega_{p,1}(q) &= \sqrt{\frac{4\ln 2}{\hbar}}\,(v_F r_s q)^{1/2}\,\sqrt{k_BT}\left\{1 - \frac{1}{2}\,\mathrm{e}^{-2qa}\right\}\,, \\
\omega_{p,2}(q) &= \frac{\Omega_p}{\sqrt{2}} + 4\ln 2\,\frac{r_s v_F}{\hbar\Omega_p}\,k_BT\,q\,\mathrm{e}^{-2qa}\,,
\end{aligned} \tag{22}$$

from which follow two uncoupled plasmon modes: the isolated plasmon dispersion for graphene and constant $\Omega_p/\sqrt{2}$ surface-plasmon frequency as $a \to \infty$.

The role of the bulk plasmon frequency Ω_p is to determine the frequency and exact behavior of the coupled plasmon modes at various temperatures. Consequently, in order to make the coupling effect observable, we must ensure that the frequencies of the two plasmon modes (surface plasmon in the conducting substrate and the plasmon and Fermi energy in the two-dimensional layer, e.g. graphene)should be of the same order of magnitude. Apart from this, we always have to keep track of the plasmon damping which appears if the collective modes enter the regions of single-partcile excitations. In this sense, the frequency Ω_p directly affects Landau damping of each mode. Bulk plasma frequency Ω_p in conductor is mainly specified by two parameters - electron density n_0 and the background dielectric constant ϵ_b.

After computing the plasmon dispersion $\omega_p(q)$, we may use the result to calculate the plasmon dissipation rate $\gamma_p(q)$ for the open system in Fig. 1. First, we need to take into account the imaginary part of the polarization function $\mathrm{Im}\,\Pi_T^{(0)}(q, \omega;\, \mu)$ from the contribution of particle hole modes. If we only consider small dissipation with $\gamma_p \ll \omega_p$, we

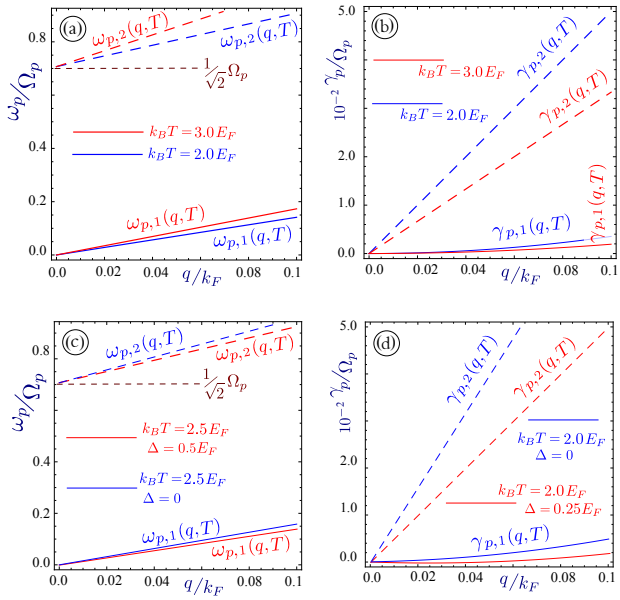

FIG. 7: (Color online) Plasmon frequencies in panels (a), (c)) and corresponding dissipation rates in (b), (d)) in the long wavelength limit for chosen T and Δ values. $\omega_{p,1}$ and $\omega_{p,2}$ in plots (a), (c), as well as $\gamma_{p,1}$ and $\gamma_{p,2}$ in plots (b), (d), correspond to lower and upper plasmon branches. The other parameters, Δ and T, are directly labeled in the figure. Here, $a = 1.0\,k_F^{-1}$ and $E_F = 10\,\mathrm{meV}$ were used in our calculations.

can neglect the very small shift of ω_p from $\backsimeq \gamma_p^2$ and $\backsimeq \gamma_p \,\mathrm{Im}\,\Pi_T^{(0)}$. Since Eq. (9) is no longer valid after introducing the graphene-conductor Coulomb coupling in the open system, we have to include both the real and imaginary parts of $\mathrm{Im}\,\Pi_T^{(0)}(q,\omega;\,\mu)$ in Eq. (19) and find the dissipation rates corresponding to each plasmon branch. We know from Eq. (18) that $\mathrm{Im}\,S_C(q,\omega;\,\mu) \backsim \mathrm{Im}\,\Pi_T^{(0)}(q,\omega;\,\mu)$, therefore, the regions of Landau damping in our open system are determined by the particle-hole modes of a graphene layer.

From Eq. (19), for $qa \ll 1$ we obtain the dissipation rate for the lower acoustic-like branch

$$\frac{\gamma_{p,1}(q)}{\Omega_p} = \frac{\pi}{4}\,(2\ln 2)^{1/2}\left(\frac{\hbar}{k_BT}\right)^{1/2}\,\frac{1}{\Omega_p}\,(r_s v_F)^{3/2}\,a^{3/2}\,q^3\ , \tag{23}$$

and that for the upper surface-plasmon-like branch

$$\frac{\gamma_{p,2}(q)}{\Omega_p} = \frac{\pi}{16\sqrt{2}}\,\hbar v_F r_s\,\frac{1}{k_BT}\,q\ . \tag{24}$$

For $qa \gg 1$, on the other hand, the dissipation rate can be approximated as

$$\begin{aligned}
\gamma_{p,1}(q) &= \frac{\pi}{8}\,\sqrt{\ln 2}\,\sqrt{\frac{\hbar}{k_BT}}\,(r_s v_F)^{3/2}\,q^{3/2}\left[1 - 8\ln 2\,\frac{r_s v_F}{\hbar\Omega_p^2}\,k_BT\,q\,\mathrm{e}^{-2qa}\right]\ , \\
\gamma_{p,2}(q) &= \frac{\pi}{16}\,\hbar\Omega_p\,\frac{r_s v_F}{k_BT}\,q\,\mathrm{e}^{-2qa}\ .
\end{aligned} \tag{25}$$

C. Gapped Graphene

In the presence of an energy gap for graphene, we expect both the plasmon frequencies and dissipation rates in the open system will be modified. From our calculation we find that the results for the plasmon frequencies are similar to those of gapless graphene except for a modified effective length Λ_Δ, i.e.,

$$\Lambda_\Delta(T) = \frac{4}{\hbar\,\Omega_p^2}\,v_F\,r_s\left\{k_BT\ln 2 - \frac{\Delta^2}{4k_BT}\left[\mathbb{C} - \ln\left(\frac{\Delta}{2k_BT}\right)\right]\right\}\ , \tag{26}$$

where $\mathbb{C}\approx 0.8$ is a small positive constant first introduced in Eq. (7). Therefore, for $qa \ll 1$ we obtain

$$\begin{aligned}\omega_{p,1}(q)/\Omega_p &= \sqrt{2a\Lambda_\Delta(T)}\,q\ ,\\ \omega_{p,2}(q)/\Omega_p &= 1/\sqrt{2} + q\Lambda_\Delta(T)/\sqrt{2}\ .\end{aligned} \tag{27}$$

In the case of $qa \gg 1$, on the other hand, the solutions are approximated as

$$\begin{aligned}\omega_{p,1}(q) &= \Omega_p\sqrt{q\Lambda_\Delta(T)}\left(1 - \frac{1}{2}\,\mathsf{e}^{-2qa}\right)\ ,\\ \omega_{p,2}(q) &= \Omega_p/\sqrt{2} + \Omega_p\,q\Lambda_\Delta(T)\,\mathsf{e}^{-2qa}\ .\end{aligned} \tag{28}$$

The calculations of the dissipation rates in the presence of an energy gap are much more complicated since they involve the modified imaginary part of the polarization function $\mathrm{Im}\,\Pi_T^{(0)}(q,\omega;\,\mu)$. A lengthy calculation for $qa \ll 1$ leads to

$$\begin{aligned}\gamma_{p,1}(q) &= \frac{\pi}{4}\,(2\ln 2)^{1/2}\left(\frac{\hbar}{k_BT}\right)^{1/2}(r_sv_F)^{3/2}\,a^{3/2}\,q^3 - \pi r_sv_Fa\Delta\left(\frac{1}{8k_BT} - \ln 2\,\frac{r_sv_F}{\hbar\Omega_p^2}\,q\right)q^2\ ,\\ \gamma_{p,2}(q) &= \frac{\pi}{16\sqrt{2}}\,v_Fr_s\,\frac{1}{k_BT}\,\left(\hbar\Omega_p - \sqrt{2}\Delta\right)q\ .\end{aligned} \tag{29}$$

We see that $\gamma_{p,1}(q)$ acquires both $\backsimeq q^3$ and $\backsimeq q^2$ terms for a finite gap, while the linear dispersions for $\gamma_{p,2}(q)$ is preserved.

IV. NUMERICAL RESULTS FOR OPEN SYSTEMS

Whenever the distance a between the 2D layer and the surface is large, these two components are decoupled. Consequently, a pair of plasmon branches one of which effectively behaves like that in the absence of the conductor, as shown in Figs. 3(a) and 3(b), except for a limited region of q. For $k_BT = 1.5\,E_F$ in these two plots, the upper branch is significantly damped. In the long wavelength limit, the Coulomb coupling is enhanced. In this case, as displayed in Figs. 3(e) and 3(f), the "dominant" (higher density peak) plasmon branch is switched to a surface plasmon-like mode approaching $\Omega_p/\sqrt{2}$ for $q \gg k_F$. This implies an enhancement of graphene-plasmon dissipation (higher brightness of density plot peak for the lower branch) for small a with an increased interaction between graphene electrons and the "external" electron reservoir in an open system, as demonstrated by comparing Fig. 3(b) with 3(f). Finally, when $k_Fa = 1.0$ in Figs. 3(c) and 3(d), these two branches are strongly coupled to each other with similar density peaks. For a closely located graphene layer from the surface, the measurement of plasmon dispersion and dissipations was reported in several recent papers [8–12]. It was discovered that if the separation becomes small enough, the lower plasmon branch is significantly damped when it enters the intraband particle-hole region. However, this plasmon dissipation is lifted up for large q, as seen from Figs. 3(e) and 3(f), due to shrinking of the intraband particle-hole region.

Even for a closed system of monolayer graphene, we are aware that the plasmon dissipation varies with temperature through the modification of intraband and interband particle-hole excitations. For our open system, we expect the graphene-conductor Coulomb coupling will further change the thermal modulation of plasmon dissipation. As an example of the temperature dependence, we present in Fig. 4 the plasmon dispersion as a function of T. For $\Delta = 0$ in panels (a)-(d), we find the energy of the upper branch (surface-plasmon like) exhibits a monotonic increase with T, and its dissipation becomes significant for large q and small a values, as seen from Fig. 4(d). The lowest dissipation is reached for small q and intermediate a values in Fig. 4(b).

Interestingly, the dissipation of the lower acoustic like branch remains very small for $q = 0.2\,k_F$ in Fig. 4(a)-(c) at all temperatures and different values of a, only exhibiting large dissipation in Fig. 4(d) for $q = 0.6\,k_F$. Temperature

dependence of plasmons with $\Delta \neq 0$ is shown in Fig. 4(e) and 4(f). Here, a small bandgap in Fig. 4(f) leads to increased dissipation for the upper branch, but this dissipation is suppressed by a large gap in Fig. 4(e).

Numerical results for the open system with a finite energy bandgap in graphene are presented in Figs. 5 and 6 for a large and small gap, respectively. For ($\Delta = 0.8\, E_F$ in Fig. 5, we find the upper branch remains undamped at large values of q at both low and high temperatures due to the gap opening between the intraband and interband particle-hole modes. Moreover, we observe that increase of T or Δ gives rise to opposite effects on the shift of plasmon energy. It is obvious from Fig. 5 that the energy gap has a profound influence on the plasmon energy and dissipation for small $q \ll k_F$, where the Coulomb coupling between graphene and the conductor becomes strong for fixed layer separation a (scaled as $qa \sim 1$). Therefore, a smaller separation a implies a larger range of q for significant variation of plasmon frequency and dissipation, as shown in Figs. 5(e) and 5(f). On the other hand, for small gap ($\Delta = 0.2\, E_F$ in Fig. 6, the major features in Fig. 3 for the gapless graphene are largely retained. However, change in the upper plasmon branch by the energy gap can still be seen especially in the small q region.

In order to get a quantitative view of both the plasmon dispersion $\omega_{p,1}(q)$, $\omega_{p,2}(q)$ and the plasmon dissipation rates $\gamma_{p,1}(q)$, $\gamma_{p,2}(q)$, results for these quantities are presented in Fig. 7 in the long wavelength limit. From Fig. 7(a) with $\Delta = 0$, we clearly see that increase in temperature will enhance the plasmon energies for both lower and upper branches. On the other hand, for fixed $k_BT = 2.5\, E_F$ it is found from Fig. 7(c) that increasing Δ leads to the reduction of linearly q-dependent plasmon energies of both branches. Furthermore, we observe from Fig. 7(b) and (d) that the plasmon dissipation rate of the lower branch ($\sim q^3$) is much lower than that of the higher branch ($\sim q$). Here, the dissipation rates of gapless graphene in the open system is reduced by increasing T. For gapped graphene in the open system, on the other hand, the increase of Δ leads to the enhancement of the plasmon dissipation rates of both branches.

V. CONCLUDING REMARKS

In summary, we have obtained analytic expressions for the plasmon dispersion relations and dissipation rates for gapped graphene at high temperature in both closed and open systems. In the presence of an energy gap 2Δ, we have found that the plasmon frequency is modified according to $\Delta^2/(4k_BT)\ln(\Delta/(2k_BT))$, which is different from the result at $T = 0$. For doped gapped graphene, we have also derived an analytical formalism for studying plasmon dispersion and dissipation in the low-temperature limit, which was not reported in previous studies.

We investigated properties of both intraband and interband particle-hole modes in doped graphene and find distinctive behaviors at high temperature for these two types of excitation. We performed numerical calculations with respect to plasmon dispersion and dissipation for an open system at finite temperature, variable doping and energy gap. When the gap is large, a novel feature in the dispersion relation of the upper surface plasmon-like branch is obtained, i.e., opposite shifts of the plasmon frequencies with respect to energy gap and temperature. For the lower acoustic-like branch, as the coupling to the conductor is very strong, dissipation is suppressed at large wave vectors due to shrinking of the intraband particle-hole region.

Our calculations have shown that as the separation between monolayer graphene and the conductor is decreased, hybridization of the surface and graphene plasmons becomes significant. Additionally, the particle-hole mode contributions are enhanced at the same time. Consequently, strong Landau damping always occurs for these two plasmon branches, except when there is a large energy gap and relatively low temperature. In comparison with the gapless graphene, the existence of energy gap reduces the plasmon dissipation, and then, stabilizes the plasmon excitations in the open system. Such a linear reduction of dissipation with respect to energy gap for the upper plasmon branch, as graphene layer is in proximity with a conductor, is absent for a free-standing graphene layer. Moreover, the dissipation of the lower plasmon branch is essentially suppressed if the energy gap is large. All of these findings confirm that the coupling to the environment will introduce additional dissipation channel for plasmons, and the magnitude of this new dissipation rate varies with the energy gap and temperature.

Acknowledgments

This research was supported by contract # FA 9453-13-1-0291 of AFRL. DH would like to thank the support from the Air Force Office of Scientific Research (AFOSR).

Appendix A: Analytical Expression for the Plasmon Dispersion in Gapped Graphene at Finite Temperatures

The energy dispersion of gapped graphene may be expressed as $\varepsilon(k) = \pm\sqrt{\Delta^2 + (\hbar v_F k)^2}$ where v_F is the Fermi velocity and 2Δ is the energy gap between the valence (-) and conduction (+) bands. At zero temperature, the polarization function in the long-wavelength limit is given by Eq. (4) Equation (4) is valid for $\Delta < \mu$. If $\Delta > \mu$, the conduction band is completely empty and only interband transitions contribute to the plasmon excitations. We may use Eq. (4) in Eq. (2) with lower limit of integration Δ to determine the polarization for finite temperatures. We have

$$\Pi_T^{(0)}(q,\omega;\,\mu) = \int\limits_{\Delta}^{\infty} d\,\mu' \frac{\Pi_{T=0}^{(0)}(q,\omega;\,\mu')}{4k_BT\cosh^2\left(\frac{\mu-\mu'}{2k_BT}\right)} = \tag{A1}$$
$$= \int\limits_{\Delta}^{\infty} d\,\mu'\ \frac{\mu'}{\pi\hbar^2}\left[1-\left(\frac{\Delta}{\mu'}\right)^2\right]\frac{q^2/\omega^2}{4k_BT\cosh^2\left(\frac{\mu-\mu'}{2k_BT}\right)}\ .$$

For intrinsic graphene with $\mu = 0$, this integral can be split into two parts, i.e., $\Pi_T^{(0)}(q,\omega;\,\mu=0) = I_1 + I_2$ with

$$I_1 \ = \ \int\limits_{\Delta}^{\infty} d\,\mu'\,\frac{\mu'}{\pi\hbar^2}\,\frac{q^2/\omega^2}{4k_BT\cosh^2\left(\mu'/2k_BT\right)} = \frac{2q^2}{\pi\hbar^2\omega^2}\left\{\frac{k_BT}{4}\ln 16 - \frac{\Delta}{2}\,\tanh\left(\frac{\Delta}{2k_BT}\right) + k_BT\ln\left[\cosh\left(\frac{\Delta}{2k_BT}\right)\right]\right\}\ ,$$
$$I_2 \ = \ -\frac{\Delta^2 q^2}{2k_BT\pi\hbar^2\omega^2}\int\limits_{\Delta}^{\infty}\frac{d\,\mu'}{\mu'}\cosh^{-2}\left(\frac{\mu'}{2k_BT}\right)\ . \tag{A2}$$

Here, we have considered the fact that, for the case of intrinsic graphene at $T \Longrightarrow 0$, the peak of the integrand occurs at $\mu' = 0$, and therefore, an extra factor of 2 is required.

For high temperatures, we approximate

$$I_1 = \frac{1}{\pi\hbar^2}\,\frac{k_BT}{2}\,\frac{q^2}{\omega^2}\,\ln 16 + \frac{2}{\pi\hbar^2}\,\frac{q^2}{\omega^2}\,G_1(T,\,\Delta)\ , \tag{A3}$$

where

$$G_1(T,\,\Delta) = k_BT\ln\left[\cosh\left(\frac{\Delta}{2k_BT}\right)\right] - \frac{\Delta}{2}\,\tanh\left(\frac{\Delta}{2k_BT}\right) \backsimeq \frac{\Delta^2}{8k_BT} - \frac{\Delta^2}{4k_BT} = -\frac{\Delta^2}{8k_BT}\ . \tag{A4}$$

As a result, we get

$$I_1 = \frac{2\ln 2}{\pi\hbar^2}\,k_BT\,\frac{q^2}{\omega^2} - \frac{1}{\pi\hbar^2}\,\frac{\Delta^2}{4k_BT}\,\frac{q^2}{\omega^2}\ . \tag{A5}$$

The remaining term is rewritten as

$$I_2 = -\frac{1}{2\pi\hbar^2}\,\frac{\Delta^2}{2k_BT}\,\frac{q^2}{\omega^2}\,G_2(T,\,\Delta)\ , \tag{A6}$$

where

$$G_2(T,\,\Delta) = \int\limits_{\Delta}^{\infty}\frac{d\mu'}{\mu'}\,\frac{1}{\cosh^2(\mu'/2k_BT)}\ . \tag{A7}$$

Here, we are looking for an approximated and analytic form for the following integral:

$$\int_{\delta}^{\infty} \frac{dx}{x\cosh^2(x)} \ , \tag{A8}$$

where $\delta = \Delta/(2k_BT) \ll 1$. In order to avoid the singularity appearing as $\delta \to 0$, we perform the integration by parts. Consequently, we obtain

$$\int_{\delta}^{\infty} \frac{dx}{x\,\cosh^2 x} = \frac{\ln x}{\cosh^2(x)}\bigg|_{\delta}^{\infty} + 2\int_{\delta}^{\infty} dx\ \frac{\ln x\ \tanh(x)}{\cosh^2(x)} \ . \tag{A9}$$

For $\delta \to 0$ or $\Delta \ll k_BT$, the first term gives

$$\frac{\ln x}{\cosh^2(x)}\bigg|_{\delta}^{\infty} = -\ln\left(\frac{\Delta}{2k_BT}\right) \ . \tag{A10}$$

The second part is a small correction since the integrand does not diverge for $\delta \to 0$, i.e.,

$$\mathbb{C}_1 = \int_{\delta}^{\infty} dx\,\frac{\ln x\ \tanh(x)}{\cosh^2(x)} \backsimeq \int_{0}^{\infty} dx\,\frac{\ln x\ \tanh(x)}{\cosh^2(x)} = \frac{1}{6}\left[36\ \ln \mathcal{A}_{GK} - 7\ln 2 - 3(1+\gamma_{Eu})\right] , \tag{A11}$$

where $\mathcal{A}_{GK} \backsimeq 1.2824$ and $\gamma_{Eu} = 0.5772$ are the Glaisher-Kinkelin and Euler-Mascheroni constants, respectively. [57] As a matter of fact, the result of integral the integral above is $\mathbb{C}_1 - \mathcal{O}(\delta^2 \log\delta)$. However, the second term can be dropped because I_2 in Eq.(A6) already includes Δ^2 in front of $G_2(T,\Delta)$ and all the higher powers of $\delta = \Delta/(2k_BT)$ become negligible.

Eventually, from a direct numerical integration we arrive at the result

$$G_2(T,\,\Delta) = \int_{\delta\ll 1}^{\infty} \frac{dx}{x\ \cosh^2(x)} \backsimeq -\ln\left(\frac{\Delta}{2k_BT}\right) + \mathbb{C}_2 > 0 \tag{A12}$$

even though $\mathbb{C}_2 = 2\mathbb{C}_1 \backsimeq -0.20$.

Finally, the polarization function take the form

$$\Pi_T^{(0)}(q,\omega;\,\mu=0) = I_1 + I_2 = \frac{2\ln 2}{\pi\hbar^2}\,k_BT\,\frac{q^2}{\omega^2} - \frac{1}{\pi\hbar^2}\,\frac{\Delta^2}{4k_BT}\left[-\ln\left(\frac{\Delta}{2k_BT}\right) + \mathbb{C}\right]\frac{q^2}{\omega^2} \ , \tag{A13}$$

where $\mathbb{C} = 1 + \mathbb{C}_2 \approx 0.8$. The finite-temperature dielectric function $\epsilon_T(q,\,\omega)$ for intrinsic gapped graphene is

$$\epsilon_T(q,\,\omega) = 1 - \frac{2\pi e^2}{\epsilon_s q}\,\Pi_T^{(0)}(q,\omega;\,\mu=0) = 1 - \frac{2\pi}{q}\,r_s\hbar v_F\,\Pi_T^{(0)}(q,\omega;\,\mu=0) \ . \tag{A14}$$

From this, we deduce the temperature-dependent plasma frequency of gapped graphene given by

$$\omega_p^2(q) = \frac{4}{\hbar}\,v_F r_s q\left\{k_BT\ln 2 - \frac{\Delta^2}{8k_BT}\left[\mathbb{C} - \ln\left(\frac{\Delta}{2k_BT}\right)\right]\right\} \ . \tag{A15}$$

---

[1] B. Wunsch, T. Stauber, F. Sols, and F. Guinea, New Journal of Physics **8**, 318 (2006).

[2] E. Hwang and S. D. Sarma, Physical Review B **75**, 205418 (2007).
[3] P. Pyatkovskiy, Journal of Physics: Condensed Matter **21**, 025506 (2009).
[4] S. D. Sarma and Q. Li, Physical Review B **87**, 235418 (2013).
[5] D. Abergel, V. Apalkov, J. Berashevich, K. Ziegler, and T. Chakraborty, Advances in Physics **59**, 261 (2010).
[6] D. H. Godfrey Gumbs, *Properties of Interacting Low-Dimensional Systems* (Wiley-VCH, 2011), isbn: 978-3-527-40894-8 ed.
[7] R. Roldán, J.-N. Fuchs, and M. Goerbig, Physical Review B **80**, 085408 (2009).
[8] A. Politano and G. Chiarello, Nanoscale **6**, 10927 (2014).
[9] A. Politano and G. Chiarello, Progress in Surface Science (2015).
[10] A. Politano, A. R. Marino, and G. Chiarello, Phys. Rev. B **86**, 085420 (2012).
[11] A. Politano, A. R. Marino, V. Formoso, D. Farías, R. Miranda, and G. Chiarello, Phys. Rev. B **84**, 033401 (2011).
[12] A. Politano, V. Formoso, and G. Chiarello, Journal of Physics: Condensed Matter **25**, 345303 (2013).
[13] A. V. Zayats, I. I. Smolyaninov, and A. A. Maradudin, Physics reports **408**, 131 (2005).
[14] A. R. Halpern, J. B. Wood, Y. Wang, and R. M. Corn, ACS nano **8**, 1022 (2013).
[15] W. Srituravanich, N. Fang, C. Sun, Q. Luo, and X. Zhang, Nano letters **4**, 1085 (2004).
[16] P. Nordlander, C. Oubre, E. Prodan, K. Li, and M. I. Stockman, Nano Letters **4**, 899 (2004).
[17] G. Gumbs, A. Balassis, A. Iurov, and P. Fekete, The Scientific World Journal **2014** (2014).
[18] G. Gumbs, A. Iurov, A. Balassis, and D. Huang, Journal of Physics: Condensed Matter **26**, 135601 (2014).
[19] A. Iurov, G. Gumbs, B. Gao, and D. Huang, Applied Physics Letters **104**, 203103 (2014).
[20] A. Balassis and G. Gumbs, Phys. Rev. B **90**, 075431 (2014).
[21] L. Zhemchuzhna, G. Gumbs, A. Iurov, D. Huang, and B. Gao, Physics of Plasmas **22**, 032116 (2015).
[22] M. S. Dresselhaus, G. Dresselhaus, and P. C. Eklund, *Science of Fullerenes and Carbon Nanotubes: Their Properties and Applications* (Academic Press, 1996), isbn-13: 978-0122218200 ed.
[23] M. F. Lin and K. W. K. Shung, Phys. Rev. B **50**, 17744 (1994).
[24] C.-C. Liu, W. Feng, and Y. Yao, Physical review letters **107**, 076802 (2011).
[25] C. J. Tabert and E. J. Nicol, Physical Review B **89**, 195410 (2014).
[26] M. Campisi, P. Hänggi, and P. Talkner, Rev. Mod. Phys. **83**, 771 (2011).
[27] M. Campisi, P. Talkner, and P. Hänggi, Phys. Rev. Lett. **102**, 210401 (2009).
[28] M. Esposito, U. Harbola, and S. Mukamel, Rev. Mod. Phys. **81**, 1665 (2009).
[29] G. E. Crooks, Journal of Statistical Mechanics: Theory and Experiment **2008**, 10023 (2008).
[30] S. Mukamel, Phys. Rev. Lett. **90**, 170604 (2003).
[31] W. De Roeck and C. Maes, Phys. Rev. E **69**, 026115 (2004).
[32] G. E. Crooks, Phys. Rev. E **60**, 2721 (1999).
[33] F. Setiawan and S. D. Sarma, arXiv preprint arXiv:1509.05067 (2015).
[34] U. Weiss, *Quantum dissipative systems*, vol. 10 (World Scientific, 1999).
[35] E. Illes, C. Roy, and S. Hughes, Optica **2**, 689 (2015).
[36] M. Silaev, T. T. Heikkilä, and P. Virtanen, Phys. Rev. E **90**, 022103 (2014).
[37] G. Schaller, *Open Quantum Systems Far from Equilibrium* (Springer, Lecture Notes in Physics, 2014).
[38] G. Gumbs, A. Iurov, and N. J. M. Horing, Phys. Rev. B **91**, 235416 (2015).
[39] S. B. Singer, M. Mecklenburg, E. R. White, and B. C. Regan, Phys. Rev. B **84**, 195468 (2011).
[40] V. V. Deshpande, S. Hsieh, A. W. Bushmaker, M. Bockrath, and S. B. Cronin, Phys. Rev. Lett. **102**, 105501 (2009).
[41] G. Tessier, M. Bardoux, C. Bou, C. Filloy, and D. Fournier, Applied Physics Letters **90**, 171112 (2007).
[42] G. Kucsko, P. C. Maurer, N. Y. Yao, M. Kubo, H. J. Noh, P. K. Lo, H. Park, and M. D. Lukin, Nature **500**, 7460 (2013).
[43] M. Mecklenburg, W. A. Hubbard, E. R. White, R. Dhall, S. B. Cronin, S. Aloni, and B. C. Regan, Science **347**, 629 (2015).
[44] O. V. Kibis, Phys. Rev. B **81**, 165433 (2010).
[45] M. Busl, G. Platero, and A.-P. Jauho, Physical Review B **85**, 155449 (2012).
[46] G. Giovannetti, P. A. Khomyakov, G. Brocks, V. M. Karpan, J. van den Brink, and P. J. Kelly, Phys. Rev. Lett. **101**, 026803 (2008).
[47] K. L. Grosse, M.-H. Bae, F. Lian, E. Pop, and W. P. King, Nature nanotechnology **6**, 287 (2011).
[48] N. Reckinger, A. Vlad, S. Melinte, J.-F. Colomer, and M. Sarrazin, Applied Physics Letters **102**, 211108 (2013).
[49] K. W. K. Shung, Phys. Rev. B **34**, 979 (1986).
[50] T. Ando, Journal of the Physical Society of Japan **75**, 074716 (2006).
[51] P. F. Maldague, Surface Science **73**, 296 (1978).
[52] Y. Baorong, K. Linghua, L. Jianhong, and H. Xiwei, Plasma Science and Technology **11**, 515 (2009).
[53] E. H. Hwang and S. Das Sarma, Phys. Rev. B **79**, 165404 (2009).
[54] N. J. M. Horing, Physical Review B **80**, 193401 (2009).
[55] A. Politano, V. M. Silkin, I. A. Nechaev, M. S. Vitiello, L. Viti, Z. S. Aliev, M. B. Babanly, G. Chiarello, P. M. Echenique, and E. V. Chulkov, Phys. Rev. Lett. **115**, 216802 (2015).
[56] D. Kepaptsoglou, D. Gilks, L. Lari, Q. Ramasse, P. Galindo, M. Weinert, L. Li, G. Nicotra, and V. Lazarov, Microscopy and Microanalysis **21**, 1151 (2015).
[57] S. E. by Eric W. Weisstein, *CRC Concise Encyclopedia of Mathematics* (Chapman and Hall/CRC, 2002).